Mycobacterium abscessus cording prevents phagocytosis and promotes abscess formation

Audrey Bernut, Jean-Louis Herrmann, Karima Kissa, Jean François Dubremetz, Jean-Louis Gaillard, Georges Lutfalla, Laurent Kremer

HAL Id: hal-02088315

https://hal.umontpellier.fr/hal-02088315

Submitted on 2 Apr 2019

Mycobacterium abscessus cording prevents phagocytosis and promotes abscess formation

Audrey Bernut[a], Jean-Louis Herrmann[b], Karima Kissa[a,c], Jean-François Dubremetz[a], Jean-Louis Gaillard[b], Georges Lutfalla[a,1], and Laurent Kremer[a,c,1]

[a]Laboratoire de Dynamique des Interactions Membranaires Normales et Pathologiques, Centre National de la Recherche Scientifique Unité Mixte de Recherche 5235, Université Montpellier 2, 34095 Montpellier, France; [b]EA3647-EPIM, Unité de Formation et de Recherche des Sciences de La Santé, Université de Versailles St Quentin, 78180 Montigny le Bretonneux, France; and [c]Institut National de la Santé et de la Recherche Médicale, Dynamique des Interactions Membranaires Normales et Pathologiques, 34095 Montpellier Cedex 05, France

Mycobacterium abscessus is a rapidly growing *Mycobacterium* causing a wide spectrum of clinical syndromes. It now is recognized as a pulmonary pathogen to which cystic fibrosis patients have a particular susceptibility. The *M. abscessus* rough (R) variant, devoid of cell-surface glycopeptidolipids (GPLs), causes more severe clinical disease than the smooth (S) variant, but the underlying mechanisms of R-variant virulence remain obscure. Exploiting the optical transparency of zebrafish embryos, we observed that the increased virulence of the *M. abscessus* R variant compared with the S variant correlated with the loss of GPL production. The virulence of the R variant involved the massive production of serpentine cords, absent during S-variant infection, and the cords initiated abscess formation leading to rapid larval death. Cording occurred within the vasculature and was highly pronounced in the central nervous system (CNS). It appears that *M. abscessus* is transported to the CNS within macrophages. The release of *M. abscessus* from apoptotic macrophages initiated the formation of cords that grew too large to be phagocytized by macrophages or neutrophils. This study is a description of the crucial role of cording in the in vivo physiopathology of *M. abscessus* infection and emphasizes cording as a mechanism of immune evasion.

morphotype | pathogenesis | granuloma | innate immunity

The rapidly growing mycobacterium (RGM) *Mycobacterium abscessus* (*M. abscessus*) is an emerging pathogen that infects a wide spectrum of tissues in humans, including lungs, skin, and soft tissues (1, 2). *M. abscessus* lung disease is highly prevalent in patients with cystic fibrosis (CF) and is becoming a major issue for most CF centers worldwide (3–6). Although *M. abscessus* is an RGM, it can persist and cause lung disease with caseous lesions (7).

M. abscessus exists as two variants: rough (R) and smooth (S). Ex vivo and in vivo studies have described the hypervirulence phenotype of the R versus the S morphotype (8, 9), and epidemiological studies have confirmed the persistence and acute respiratory syndromes caused by the R morphotype (4, 10, 11). The major difference between the R and S variants is the loss of a surface-associated glycopeptidolipid (GPL) (12). Analysis of the pathogenicity of *M. abscessus* has been hampered by the lack of genetic tools and the restricted panel of cellular/animal models. However, new genetic tools, including conditional gene expression, recently have been applied to both the S and R morphotypes (13, 14), but developing new animal models amenable to the manipulation of the host response is still challenging. The *M. abscessus* genome harbors a mercury-resistance plasmid sharing 99% identity with an episome from the slow-growing fish pathogen *Mycobacterium marinum*, indicating that these species have exchanged this plasmid in a shared ecosystem (15). *M. abscessus* has been described in wild and captive fish species (16, 17), and hand infections caused by *M. abscessus* have been reported in healthy fish handlers (18), suggesting a possible transmission from fish to human.

The zebrafish (ZF) is rapidly gaining favor as a useful model for the study of host–bacterial interactions (19–25). Because of its genetic tractability and optical transparency, ZF embryos represent an exquisite model to study many aspects of infectious diseases. Although adult ZF have a complex immune system similar to that of humans, with both innate and adaptive immunity, embryos and early larvae harbor only innate immunity, allowing analysis of the role of this arm of immunity during the development of mycobacterial infections (19, 21). The study of *M. marinum*-infected ZF embryos has brought remarkable insights into the understanding of human tuberculosis (19, 26), such as the specific role of eicosanoids in host defense (27), the role of macrophages in pathogen dissemination (28), infection-induced antibiotic tolerance (29), and the contribution of the type VII secretion system (ESX) in granuloma formation (30). Importantly, conserved virulence mechanisms and host susceptibility determinants identified during ZF infection have been validated in *Mycobacterium tuberculosis* and human susceptibility (27). Therefore we reasoned that ZF also may represent a useful experimental model to decipher the pathogenicity of *M. abscessus* and the immunopathology of *M. abscessus* infections.

We developed the ZF embryo as a tractable model for the study of systemic *M. abscessus* infections and compared the virulence and physiopathology of S versus R morphotypes. We describe the very aggressive and lethal infections caused by the R morphotype, which forms serpentine cords and unexpected infections of the central nervous system (CNS). This in vivo study

Significance

Mycobacterium abscessus is the most frequently isolated rapidly growing mycobacterium in human disease and recently has emerged as responsible for severe pulmonary infections in cystic fibrosis patients. However, little is known about the virulence mechanisms of this human pathogen. We adapted the zebrafish embryo as a tractable infection model to study, at a spatiotemporal level, the physiopathology of *M. abscessus* infection. We describe the high propensity of virulent rough variant *M. abscessus* to produce serpentine cords in vivo, which are not observed with the less virulent smooth variant. We demonstrate that extracellular cording allows the bacterium to withstand phagocytosis, leading to uncontrolled growth and establishment of an acute and lethal infection, thus constituting a determinant of virulence.

demonstrates how the formation of cords allows this RGM to escape the immune system.

Results

Rough *M. abscessus* Are More Virulent than Smooth *M. abscessus* in ZF.

Bacterial suspensions of S- and R-variant *M. abscessus* CIP104536[T] were injected into the caudal vein of embryos at 30 h post fertilization (hpf) (Fig. S1). Most embryos injected with the S morphotype were still alive at 13 d post infection (dpi) (Fig. 1*A*). In sharp contrast, about 50% of embryos injected with the R morphotype were dead at 8 dpi, and 60–70% of the larvae died before 13 dpi. Injection of large amounts of S bacteria failed to induce larval mortality, whereas injection of higher infectious doses of the R variant resulted in earlier embryo death (Fig. 1*B*).
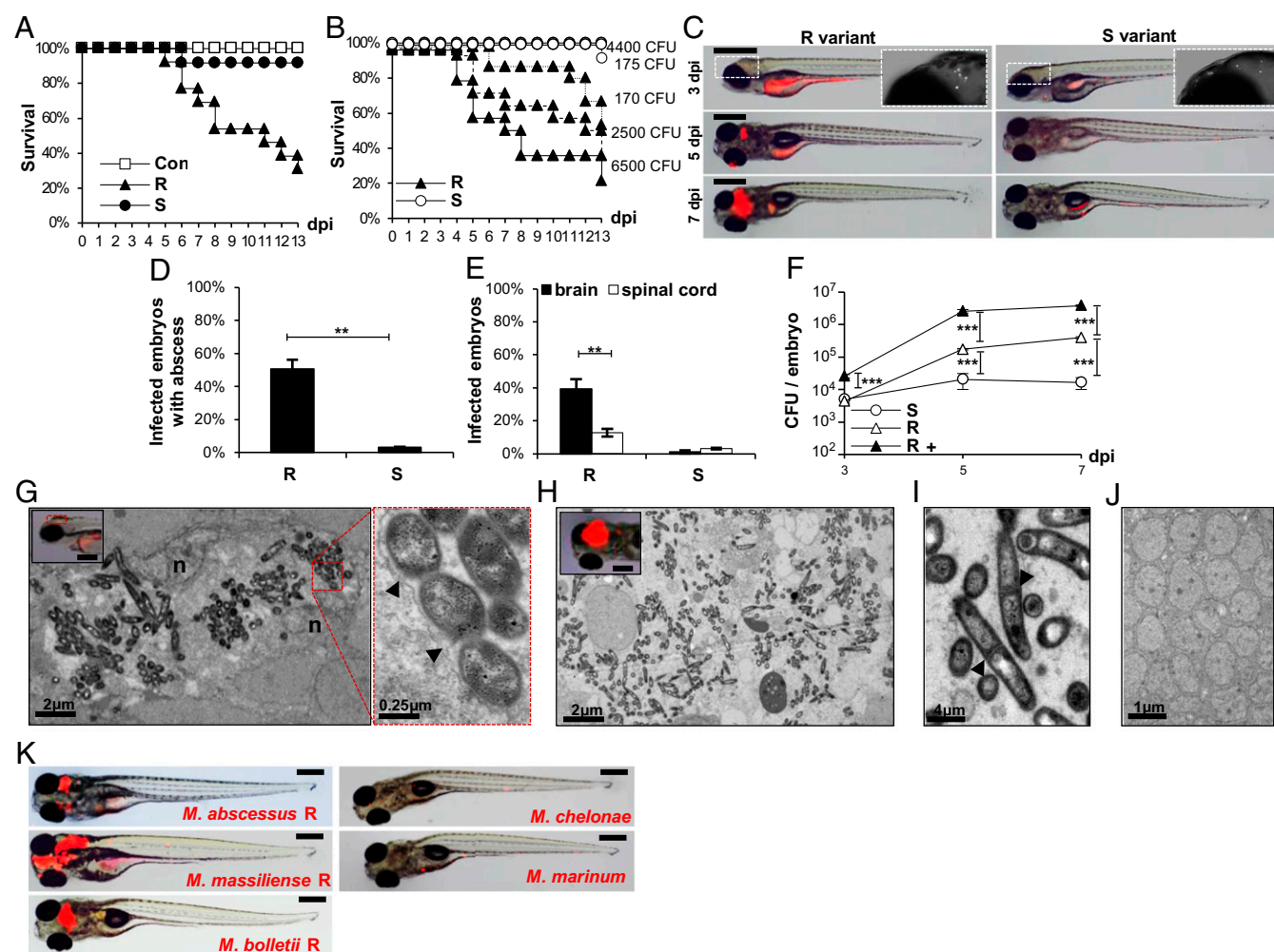

Fig. 1. Increased virulence and specific neurotropism of rough *M. abscessus* in ZF embryos. (*A*) Survival of embryos infected with ∼300 colony forming units (cfu) of the *M. abscessus* R or S variant compared with mock-infected controls (Con) (*n* = 20). Shown are representative results of three independent experiments. Embryos are significantly more susceptible to R-variant infection (*P* < 0.0001, log-rank test) than S-variant infection (statistically not different from mock-infected control). (*B*) Survival curves of embryos infected at various doses of *M. abscessus* R or S variant. Data shown are representative of two independent experiments; *n* = 20. Survival of embryos infected with the R variant depends on the dose (*P* < 0.0001, log-rank test). No statistically significant difference is seen between the control group and the embryos injected with the S variant, regardless of the dose. (*C*) Spatiotemporal visualization of the infection by either the R or the S variant expressing mCherry (∼300 cfu): representative fluorescence and transmission overlay of whole embryos and close-up of the brain. The yolk is auto-fluorescent. (Scale bars, 400 μm.) (*D*) Frequency of R- and S-variant abscesses in whole embryos over 13 dpi (∼300 cfu; *n* = 40, three independent experiments). (*E*) Average localization of abscesses of the infected embryos in *D*. Embryos infected with the R variant developed more abscesses within the brain or the spinal cord than embryos infected with the S variant (*P* < 0.001). (*F*) Bacterial loads of embryos infected with the R or S variant (∼200 cfu). Embryos infected with the R variant were separated into two groups, with (R+) or without (R) abscesses. Results are expressed as mean cfu per embryo from three independent experiments. Significant expansion of bacterial loads was observed up to 5 dpi within embryos infected with the R or the S variant (*P* = 0.001). Except for the bacterial load at 3 dpi in embryos infected with the R variant without abscess and embryos infected with the S variant, the bacterial burdens were significantly different between each group and at each time point. (*G–J*) DIC and fluorescent overlays of 3-dpi (boxed in *G*) and 7-dpi (boxed in *H*) embryos used for the TEM analysis of brain infection in embryos infected with the R variant (Scale bars, 200 μm). (*G*, *H*, *I*, and *J*). Representative electron micrographs show a transverse section through the brain of embryos infected with the R variant at 3 dpi (*G*) and 7 dpi (*H–J*). (*G*) Two macrophages with intracellular bacteria internalized into multiple phagosomes present in the boxed infection area are shown. n, nucleus. Close-up view of one phagosome showing the membrane of phagosomal compartment (arrowheads). (*H*) TEM image of a typical brain lesion (boxed) with extensive extracellular bacterial replication and cellular debris. (*I*) Bacterial division. Arrowheads indicate division septum. (*J*) Healthy brain tissue. Significance was assessed by a generalized mixed-effects model fitted with a binomial (*D* and *E*) or Poisson distribution (*F*), comparing the proportion of both strains in each category. **P* < 0.01; ****P* < 0.001. Error bars represent the SD. (*K*) *Golden* embryos *i.v.* infected by several mycobacterial species expressing mCherry. Representative fluorescence and DIC overlay of R variants of *M. abscessus* complex members (*M. abscessus senso stricto*, *M. massiliense*, and *M. bolletii*), *M. chelonae*, or *M. marinum* infections in whole infected embryos at 5 dpi. (Scale bars, 400 μm.)

M. abscessus Exhibits Specific Neurotropism. Time-lapse imaging of *M. abscessus* R-infected embryos revealed growing foci of infection in the larval brain at 3 dpi (Fig. 1*C*). Embryos harboring an abscess similar to the one shown at 7 dpi in Fig. 1*C* died within the next 24 h. Over 13 dpi, abscesses were detected in 50% of R-infected embryos (Fig. 1*D*). Around 40% of infected embryos developed abscesses in the brain (Fig. 1*E*), and 15% had abscesses within the spinal cord (Fig. 1*E* and Fig. S2). The less virulent *M. abscessus* S phenotype induced abscesses only marginally (Fig. 1 *C* and *D*). The bacterial load of the *M. abscessus* S variant in infected embryos increased only slightly after infection, reaching a plateau at 5 dpi (Fig. 1*F*), whereas bacterial loads of the R variant increased exponentially by 1.5 log from 3 dpi to 5 dpi. This active replication was highlighted in embryos with abscesses in the CNS compared with those without any abscess (Fig. 1*F*). Abscesses were restricted mainly to the CNS. Overall, these data indicate that the R, but not the S, variant, induces a very robust and lethal infection in the CNS. The development of brain (Fig. 1 *G–J*) and spinal cord (Fig. S3) infections was studied further in R-infected embryos by using transmission electron microscopy (TEM). At early stages, aggregated bacilli were observed inside macrophages, surrounded by a phagosomal membrane (Fig. 1*G*). Later stages were characterized by extensive replication of extracellular bacteria (Fig. 1 *H* and *I*), leading to abscesses and tissue damage (Fig. 1 *H* and *J*).

Clinical isolates of *M. abscessus* recently have been assigned to three species on the basis of the *rpoB* sequence: *M. abscessus sensu stricto*, *M. abscessus bolletii*, and *M. abscessus massiliense* (31, 32). Infection of embryos with rough strains of *M. massiliense* or *M. bolletii* led to abscesses within the CNS, similar to those found in *M. abscessus* (Fig. 1*K*). In contrast, neither *Mycobacterium chelonae*, an RGM highly related to *M. abscessus*, nor *M. marinum* produced abscesses within the CNS, indicating that neurotropism is specific to the *M. abscessus* complex.

Cording Initiates Abscess Formation Within the CNS. Only the R variant displayed a rough and dry texture and organized serpentine cords when grown on agar (12, 14, 33) and large bacterial clumps consisting mainly of cords in liquid cultures (Fig. 2*A*). Confocal microscopy showed the presence of serpentine cords within the brain and spinal cord of an embryo infected with the R morphotype (Fig. 2 *B* and *C*). 3D analysis (Fig. 2*B*, *Right* and Movie S1) revealed highly organized structures of variable size but often larger than 100 μm. Cords appeared within 1 dpi, and the proportion of embryos with cords increased at 2 dpi (Fig. 2*D*). At this stage, ~60% of the embryos contained cords, and this proportion remained constant until 3 dpi. Cords were never observed in embryos infected with the *M. abscessus* S variant (Fig. 2*D*). The absolute number of cords per embryo increased progressively with time to an average of three cords at 3 dpi (Fig. 2*E*); cords were found mainly within the CNS and the eyes (Fig. 2*F*). The proportion of cords in the vasculature remained constant between 1 and 3 dpi (Fig. 2*F*), and their size rarely exceeded 10 μm. Interestingly, cords within the same infected individual that were imaged at 2 and 3 dpi showed a rapid and impressive growth in size and surface extension within the brain and the spinal cord, initiating the development of abscesses (Fig. 2*G*). A close-up reveals that the rapid extracellular bacterial replication led to an abscess with extrusion of both mycobacteria and host tissues.

Disruption of *mmpL4b* in the S Morphotype Correlates with High Virulence Levels in Infected ZF. Multiple genetic lesions have been reported to be associated with the loss of synthesis or transport of GPLs in R-variant *M. abscessus* (34). To address the possible link between pathogenicity and cording clearly, we used a mutant (Δ*mmpL4b*) in which *mmpL4b* was disrupted in an S variant, leading to the loss of GPLs and conversion to an R morphotype (14) with bacterial cording (Fig. 3*A*). Infectious
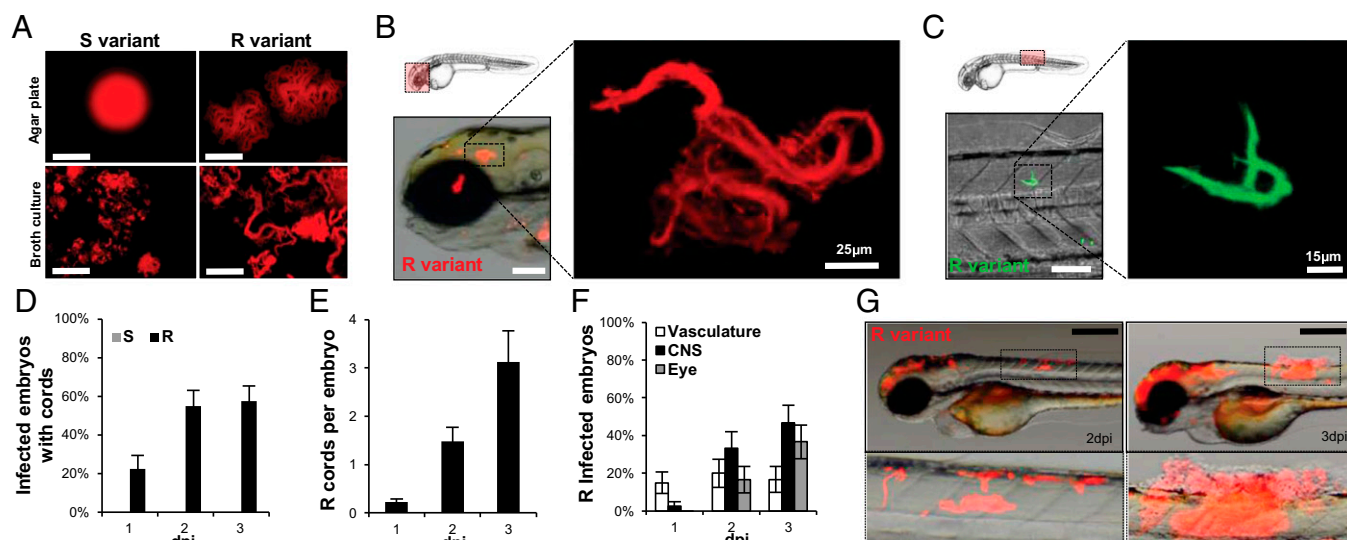
Fig. 2. In vivo cording of the R variant initiates abscess formation. (*A*) Fluorescent images of R or S morphotypes on 7H10 agar plates or 7H9/OADC/Tween broth. The S variant appears hemispherical and smooth, whereas the R variant displays serpentine cords. Only rough bacteria produce multicellular cords. (Scale bars, 1 mm.) (*B* and *C*) R-variant–infected embryos expressing mCherry (*B*) or GFP (*C*) at 2 dpi. (*B*) Fluorescence and DIC overlay of the head. (Scale bar, 150 μm.) The enlarged view at right shows a maximum intensity projection of confocal imaging of a serpentine cord. (*C*) Fluorescence and DIC overlay of part of the tail. (Scale bar, 100 μm.) The enlarged view at right shows a maximum intensity projection of confocal imaging of cords within the spinal cord. (*D*) Kinetic of cord formation in infected embryos (~300 cfu of *M. abscessus* S or R variant; n = 40). Only embryos infected with the R variant develop serpentine cords (*P* < 0.001 at each time point). The number R-variant–infected embryos with cords increased significantly up to 2 dpi (*P* = 0.03). (*E*) Average number of R-variant cords per embryo in *D*. The number of cords within R-variant–infected embryos increased significantly up to 3 dpi (*P* < 0.002). (*F*) The average localization of R-variant cords in *D*. Overall, the number of embryos with cords within the CNS and eyes increased significantly up to 3 dpi (*P* < 0.001 and *P* = 0.008, respectively). There was a significant difference in the localization of cords within embryos (*P* = 0.0008). (*G*) Abscess formation in an embryo infected with the *M. abscessus* R variant. (Scale bar, 200 μm.) Statistics were calculated using a generalized mixed-effects model fitted with a Poisson distribution (*D* and *E*) or a binomial distribution (*F*), comparing the proportion in each category across both strains. All results are expressed as the average from three independent experiments; error bars represent the SD.

MICROBIOLOGY

challenge of ZF embryos with the Δ*mmpL4b* mutant was associated with rapid killing and enhanced cording within the CNS, as seen with the wild-type R variant (Fig. 3 *B* and *C*). Small abscesses were observed within the brain as early as 3 dpi after infection with the Δ*mmpL4b* mutant (Fig. 3*D*), and, as with the R strain, grew rapidly in size until 5 dpi. About 50% of Δ*mmpL4b*-infected embryos developed abscesses (Fig. 3*E*), mostly within the brain and the spinal cord (Fig. 3*F*). Introduction of a functional *mmpL4b* copy restored both GPLs production at the bacterial surface (35) and smooth morphotype (Fig. 3*A*). Infection with the complemented strain showed no larval killing, and abscesses were al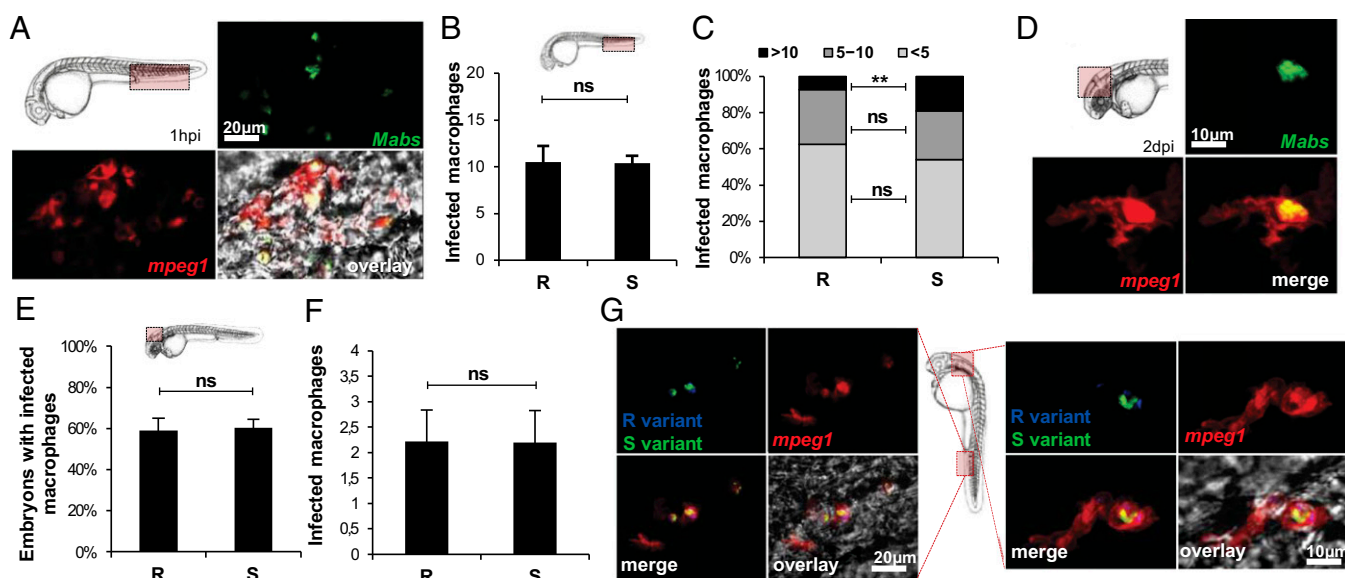most completely absent, similar to infections with the parental S strain (Fig. 3 *C*, *E*, and *F*). These results demonstrate a clear association between GPL production, in vivo cording, and *M. abscessus* pathogenicity.

***M. abscessus* S and R Variants Are Rapidly and Equally Phagocytosed by Macrophages.** Phagocytosis of GFP-labeled *M. abscessus* was analyzed after injection in tg(*mpeg1:mCherry*) embryos. Bacteria were found within macrophages close to the injection site at 1 h post infection (hpi) (Fig. 4*A*), indicating that phagocytosis occurred very rapidly. The number of infected macrophages harboring either R- or S-variant bacteria was counted in the entire region posterior to the urogenital opening. R- and S-variant bacteria were equally well phagocytosed, with an average number of 10 *M. abscessus*-containing macrophages per embryo (Fig. 4*B*). Each macrophage then was individually scored for the number of intracellular bacteria. In each embryo, the proportion of lightly infected (fewer than five bacteria), moderately infected (5–10 bacteria), and heavily infected (>10 bacteria) macrophages was determined (Fig. 4*C*). For both variants, most macrophages fell into the low-burden category, and the main difference between the R and S variants was a higher percentage of heavily infected macrophages after infection with *M. abscessus* S.

By 2 dpi, *M. abscessus*-loaded macrophages were scattered throughout tissues, including the brain (Fig. 4*D*), suggesting that macrophages can transport the pathogen to the CNS. At 1 dpi with either the S or R variant, ~60% of the embryos contained an average of two infected macrophages in the brain (Fig. 4 *E* and *F*), indicating that macrophages can disseminate S and R variants at similar rates. It remains possible that the difference in CNS pathology is dependent on the R and S variants that are taken up by different macrophage populations. Perhaps R variants were phagocytosed by macrophages destined to migrate to the brain and differentiate into microglial cells, whereas peripheral macrophages preferentially phagocytize S variants. To investigate this possibility, coinfection studies in tg(*mpeg1:mCherry*) embryos were performed with red-fluorescent R-variant (shown here in blue) and green-fluorescent S-variant bacilli. Fig. 4*G* clearly indicates that macrophages can indiscriminately phagocytose/transport S- and R-variant bacteria simultaneously. In addition, granuloma-like formation was minimal at 1 dpi, but at 2 dpi infected macrophages started forming organized granuloma-like aggregates (Fig. S4*A*). Neutrophils subsequently were recruited to the nascent granuloma (Fig. S4*B*). At 3 dpi, up to 80% of embryos contained granulomas, with no significant differences between the R and S variants (Fig. S4*C*).

Macrophages Are Required to Disseminate *M. abscessus* into the Host Tissues and to Restrict Mycobacterial Cording. The role of macrophages was investigated by using two strategies to generate macrophage-depleted embryos. First, a chemical approach was applied by injecting clodronate-impacted liposomes (Lipo-C) (36) into the caudal vein of embryos at 24 hpf. As shown in Fig. S5, the absence of red fluorescent macrophages in Lipo-C–injected tg(*mpeg1: mCherry/mpx:egfp*) embryos had no effect on the neutrophilic population, validating the efficacy of this chemical approach to deplete macrophages specifically, but not neutrophils. Images of whole embryos and cfu counts at 2 dpi indicated that Lipo-C–treated tg(*mpeg1:mCherry*) embryos infected with either the R or S variant had a massive increase in bacterial load (Fig. 5 *A* and *B*)

Fig. 3. Loss of *mmpL4b* confers high pathogenicity to the S variant. (*A*) Fluorescent pictures showing the general aspect of the S variant *M. abscessus* Δ*mmpL4b* mutant (SΔ*mmpL4b*) and its complemented strain (SΔ*mmpL4b*_C) on 7H10 agar or in 7H9/OADC/Tween broth medium. Hemispherical, smooth colonies are characteristic of SΔ*mmpL4b*_C, whereas the SΔ*mmpL4b* strain forms serpentine cords. (Scale bars, 0.5 mm.) (*B*) Fluorescence and DIC overlay of the whole head of infected embryos with red fluorescent SΔ*mmpL4b* showing large numbers of serpentine cord within the brain. (*C*) Survival of embryos infected with ~200 cfu *M. abscessus* R variant, S variant, SΔ*mmpL4b*, or SΔ*mmpL4b*_C (n = 30–40 per group). Shown are representative results from two independent experiments. Embryos are significantly more susceptible to infection by the SΔ*mmpL4b* mutant and the R variant than by the parental *M. abscessus* S variant ($P < 0.0001$, log-rank test). Complementation restored attenuation (no statistically significant differences were seen in the survival of embryos infected with SΔ*mmpL4b*_C and the embryos injected with the *M. abscessus* S variant. (*D*) Evolution of the infection by SΔ*mmpL4b* (~200 cfus) expressing mCherry. (Scale bars, 400 μm.) (*E*) Frequency of abscesses at 13 dpi (~200 cfus; n = 30–40 per group; data shown are the average of two independent experiments). *$P = 0.03$; ns, not significant. (*F*) Average localization of mycobacterial abscesses in embryos from *E*. Overall, SΔ*mmpL4b*-infected embryos developed more abscesses within the brain or the spinal cord than embryos infected with the S variant or SΔ*mmpL4b*_C ($P < 0.005$) but did not develop more abscesses than embryos infected with the R variant. A generalized mixed-effects model fitted with a binomial distribution was used for statistics in *E* and *F*. Error bars represent the SD.

that resulted in 100% larval killing at 3 dpi (Fig. 5*C*). In contrast, injection of Lipo-PBS, a nonactive derivative of Lipo-C, had no effect, and injection of Lipo-C alone in the absence of bacteria did not alter larval survival (Fig. 5*C*). These findings suggest that macrophages are instrumental for the embryos to control *M. abscessus* infections. These results were confirmed

Bernut et al.

Fig. 4. Macrophages rapidly phagocytize bacteria with no preference for S or R variants. *M. abscessus* (~100 cfu) expressing GFP (green; *A* and *D*) or tdTomato (*B*, *C*, *E*, and *F*) were injected in tg(*mpeg1:mCherry*) embryos. (*A*) Maximum intensity projection of macrophage-phagocytosed bacteria close to the injection site. (*B*) Number of individual infected macrophages at the injection site (2 hpi; *n* = 30) as counted in the displayed region (boxed area, *Upper Left*). (*C*) Average proportion of macrophages containing fewer than five, 5–10, or >10 bacteria within infected embryos in *B*. The number of individual infected macrophages with >10 bacteria is significantly greater in S-variant–infected embryos than in R-variant–infected embryos. (*D*) Confocal fluorescence of a maximum intensity projection of a *M. abscessus*-infected macrophage within the brain. (*E* and *F*) Infected macrophages found within the brain of tg(*mpeg1: mCherry/kdr:egfp*) embryos (red macrophages; green vasculature) infected with *M. abscessus* expressing tdTomato (~100 cfu) (*n* = 30). (*E*) Frequency of either R-variant– or S-variant–infected macrophages at 1 dpi as counted in the displayed region (*Inset*). (*F*) Number of individual infected macrophages within the brain of infected embryos in *E*. (*G*) tg(*mpeg1:mCherry*) embryos injected with *M. abscessus* expressing GFP and tdTomato. DIC microscopy and confocal fluorescence of maximum intensity projection of R/S-coinfected macrophages at the infection site (4 hpi, *Left*) and the brain (1 dpi, *Right*). Significance was assessed by a generalized mixed-effects model fitted with a binomial distribution (*C* and *E*) or a Poisson distribution (*B* and *F*) comparing the proportion in each category across both strains. **$P < 0.01$; ns, not significant. All results are expressed as averages of three independent experiments; error bars represent the SD.

by injecting antisense morpholinos against the myeloid transcription factor gene *pu.1* (37). Morphant embryos infected with either the *M. abscessus* R or S variant displayed heavy bacterial burdens (Fig. S6C), and survival curves of *pu.1* were very similar to those obtained following Lipo-C injection (Fig. S6 A–C). These results indicate that macrophages are required to control *M. abscessus* growth and virulence.

Even in the absence of macrophages, and despite invasive infection, S variants were not able to produce cords. In Lipo-C–injected embryos, S variants replicated actively as bacterial aggregates (Fig. 5D) that seemed restricted to blood vessels and were morphologically different from the cord-forming R variant (Fig. 5D). To test whether the *M. abscessus* R variant had access to deeper tissues, red-fluorescent bacteria were injected in the bloodstream of control tg(*kdr:egfp*) ZF (Fig. 5E), which have a GFP-labeled vasculature. The absence of colocalization indicated that a significant number of bacteria (or cords) are extravascular and have migrated into tissues (Fig. 5E); sometimes vascular obstruction and even rupture of the endothelial vasculature with cord extrusion was observed (Fig. S7A). In contrast, in macrophage-depleted embryos, R-variant cords colocalized with the endothelium vasculature (Fig. 5F, Fig. S7B, and Movie S2), suggesting that these bacteria could not egress the vascular endothelium. Similar observations were made with respect to the *M. abscessus* S variant (Fig. S7 C and D). Thus, macrophages were required for tissue dissemination of *M. abscessus* S and R variants from the vascular endothelium. Lack of macrophages was accompanied by unrestricted cording in the vasculature in all R-infected embryos, even at 1 dpi (Fig. 5G), supporting the view that macrophages can limit *M. abscessus* cording under normal conditions.

Bacteria Released from Apoptotic Macrophages Grow Extracellularly and Form Cords. The results described above indicated that macrophages restrict cording and suggest that infected macrophages are the source of *M. abscessus* from which extracellular cords may emerge. To evaluate macrophage apoptosis in infected ZF, acridine orange (AO) staining was used to differentiate apoptotic from nonapoptotic infected macrophages within the caudal vein (Fig. 6A). We observed a significant increase in the proportion of apoptotic macrophages in R-infected ZF compared with S-infected ZF at 2 and 3 dpi (Fig. 6B). This result suggests that R-infected macrophages are more susceptible to undergo apoptosis than S-infected macrophages, so that the proportion of cells heavily infected with the R variant is reduced compared with the S variant (Fig. 4C).

Importantly, during the early stage of infection (2 dpi), cellular aggregates containing both living and apoptotic macrophages were found near *M. abscessus* cords (Fig. 6C). TEM showed that later stages of infection are characterized by the presence of extracellular bacteria in an area containing cellular debris and numerous apoptotic nuclei (Fig. 6D). Thus, macrophage apoptosis could represent a key event for the release of extracellular bacteria and initiation of cord formation. Therefore, fluorescence microscopy was used to follow the evolution of infected macrophages within the eye after i. v. infection with *M. abscessus* R expressing tdTomato fluorescent protein in tg(*mpeg1:mCherry*) ZF (Fig. 6E). Individual infected macrophages are present at 1 dpi, and small cords were visible at 2 dpi, strongly suggesting that the cords originated from the infected macrophages and developed progressively for the next 24 h to generate massive cording within the eye.

Cording Prevents *M. abscessus* from Being Phagocytosed. We reasoned that the extremely large size of cords, compared with the size of most phagocytic cells, might prevent *M. abscessus* from
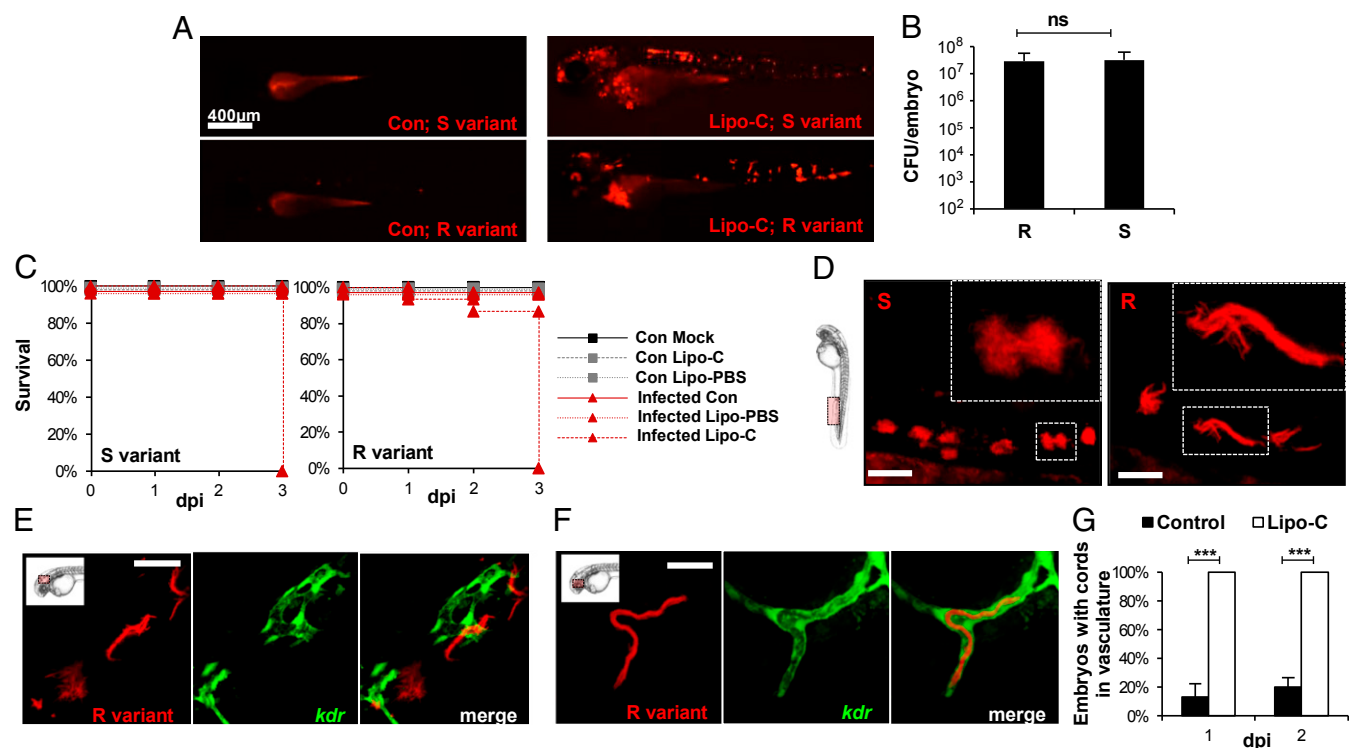
Fig. 5. *M. abscessus* infection is exacerbated and is constrained within the vasculature in the absence of macrophages. (*A*) Whole control embryos and Lipo-C–injected embryos infected with either the S (*Upper*) or the R (*Lower*) variant (tdTomato, ∼300 cfu) at 2 dpi. (*B*) Bacterial loads within Lipo-C–injected embryos infected with either the R or the S variant (∼300 cdu) at 2 dpi. (*C*) Survival curves of S- (*Left*) or R- (*Right*) infected control (con) and Lipo-C–injected embryos (∼300 cfu, n = 20). Embryos treated with Lipo-C are hypersusceptible to both *M. abscessus* variants (*P* < 0.0001, log-rank test). Shown are representative results from two independent experiments. (*D*) Confocal fluorescence microscopy of embryos injected with Lipo-C and infected with the R or S variant at 2 dpi. (*Insets*) Morphology of extracellular replicating S- and R-variant bacteria within the vasculature. In the absence of macrophages, the S variant produces clumps that are clearly different from the serpentine cords induced by the R variant (tdTomato). (Scale bars, 400 μm.) (*E* and *F*) Control (*E*), or Lipo-C–injected (*F*) tg(*kdr:egfp*) embryos infected with the tdTomato-expressing R variant (2 dpi). Control embryos show bacteria within the brain that do not colocalize with green fluorescent vasculature, whereas cords colocalize perfectly with the vasculature in the Lipo-C–infected embryo. (Scale bars, 50 μm in *E*; 30 μm in *F*.) (*G*) Frequency of cord formation in the vasculature-infected control and Lipo-C–injected embryos (n = 30, three independent experiments). Significance was assessed by a generalized mixed-effects model fitted with a binomial distribution (*G*) or a Poisson distribution (*B*), comparing the proportion in each category across both strains. ***P < 0.001; ns, not significant.

being internalized. This possibility was investigated first by injecting green fluorescent *M. abscessus* R variant into the tg (*mpeg1:mCherry*) ZF, which have red fluorescent macrophages. Confocal microscopy revealed that, although *M. abscessus* were phagocytized rapidly by macrophages (Fig. 7*A*, *Left*), bacterial cords, which were much larger in size than individual macrophages, were never found contained within these cells (Fig. 7*A*, *Right*). Because neutrophils typically are the first responders against invading pathogens, we also addressed whether these cells have the capacity to phagocytose *M. abscessus*. When injected into tg (*mpx:egfp*) embryos, which have green fluorescent neutrophils, *M. abscessus* could be found internalized in these cells (Fig. 7*B*, *Left*), indicating that neutrophils can phagocytize *M. abscessus*. However, as with macrophages, neutrophils were unable to surround and internalize the extremely long bacterial cords (Fig. 7*B*, *Right*). Therefore, mycobacterial cording appears to prevent phagocytosis and thereby promotes extracellular replication that results in the formation of abscesses and tissue damage.

Discussion

M. marinum has been extensively scrutinized in ZF, yielding important insights into tuberculosis that have had immediate clinical applications (26). We have used the ZF model to dissect the steps in the pathogenesis of *M. abscessus* directly and noninvasively. Genetic manipulation of both the pathogen and the host was used to decipher the complex interplay between *M. abscessus* and host phagocytes, starting from their earliest encounter. We demon-

strate here that ZF embryos, exhibiting only innate immunity, represent a host susceptible to the *M. abscessus* R variant but not to the *M. abscessus* S variant. By chemically depleting macrophages, we showed that, although macrophages curtail mycobacterial growth, they simultaneously allow *M. abscessus* to establish a systemic infection by promoting dissemination to deeper tissues.

The pathophysiological events of *M. abscessus* R, illustrated in Fig. 8, can be summarized as follows: (*i*) *M. abscessus* are engulfed rapidly by macrophages (and to a lesser extent by neutrophils) at the injection site; (*ii*) recruitment of macrophages leads to granuloma formation, and infected macrophages migrate from the vasculature to the CNS; (*iii*) apoptosis of infected macrophages releases bacilli, allowing their replication as extracellular serpentine cords; (*iv*) large cord structures prevent *M. abscessus* from being phagocytosed by macrophages and neutrophils. Because the cords cannot be phagocytosed, uncontrolled bacterial multiplication leads to abscess formation, tissue damage, and death.

Although some data are reminiscent of infections with *M. marinum* (37), the pathophysiological events of *M. abscessus* infections differ strikingly from those of *M. marinum*. First, the time-course of death induced by *M. abscessus* is more rapid than with *M. marinum*, with up to 50% of embryos dying 5–7 dpi and 100% within 2 wk post infection (19, 24, 38). Second, despite the apparent lack of the ESX-1 secretion system, *M. abscessus* induces granuloma formation. In *M. marinum*, this secretion system responsible for exporting the effector proteins ESAT-6 and CFP-10
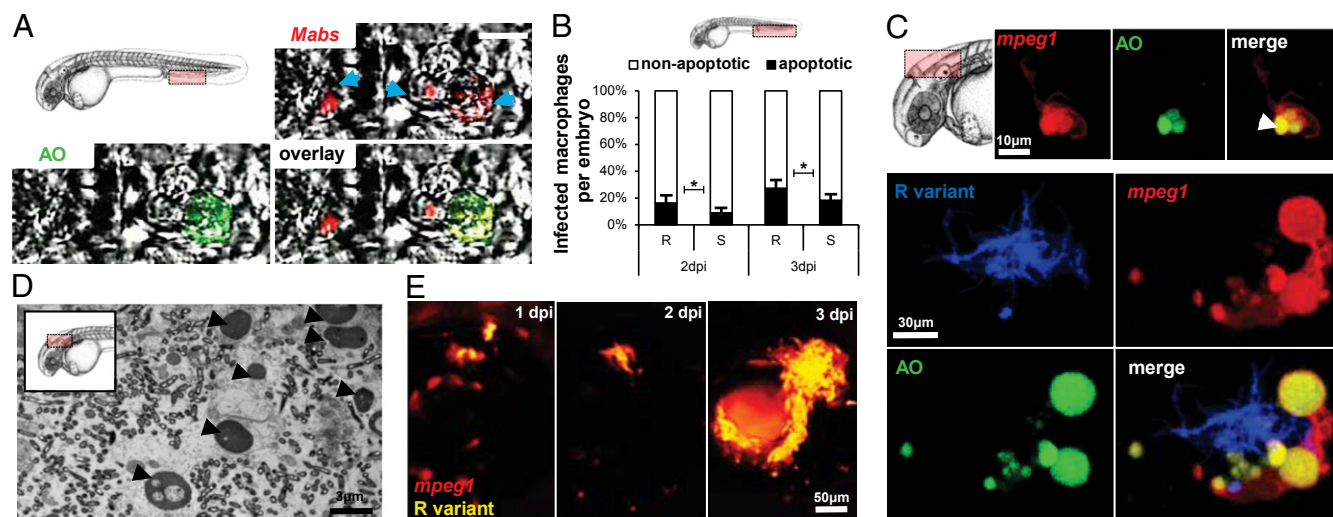
Fig. 6. Apoptosis of infected macrophages releases bacteria. (*A* and *B*) AO (green) staining of apoptosis cells in living (*A* and *C*) or fixed (*B*) infected embryos. (*A*) Representative single confocal planes fluorescence and DIC overlay of three individual macrophages (blue arrows) infected with tdTomato *M. abscessus* (red). (*Inset*) AO labeling (green) shows the presence of one *M. abscessus*-infected apoptotic cell in the vasculature of a 3-dpi embryo. (Scale bar, 10 μm.) (*B*) Proportion of apoptotic infected macrophages compared with the number of nonapoptotic infected macrophages at the infection site at 2 and 3 dpi [~300 cfu of the *M. abscessus* R or S variant injected in tg(*mpeg1:mCherry*) embryos as counted in the region displayed in the *Inset*]. Results are expressed as the averages of three independent experiments; error bars represent the SD. Significance was assessed by one-way ANOVA. (*C*) (*Upper*) Maximum intensity projection of confocal images with a representative apoptotic noninfected macrophage with apoptotic bodies (arrowhead). (*Lower*) tg(*mpeg1:mCherry*) embryos infected with R variant *M. abscessus* (tdTomato). Maximum intensity projection of confocal images show a serpentine cord (blue) surrounded by several macrophages (red) with apoptotic bodies (green) at 3 dpi. (*D*) Representative electron micrograph shows extracellular bacteria surrounded by cellular debris and typical apoptotic nuclei (arrowheads) at 7 dpi. (*E*) Spatiotemporal visualization of cord formation emerging from a macrophage infected with the R variant expressing mCherry in tg(*mpeg1:mCherry*) embryos.

is required for efficient granuloma formation in ZF embryos (30). The *M. abscessus* genome contains three ESX systems, but all are similar to the essential and highly immunogenic ESX-3 gene cluster of *M. tuberculosis* (15). Whether these gene clusters participate in *M. abscessus*-induced granulomas remains to be addressed.

Another unexpected difference is the neurotropism of *M. abscessus*, *M. massiliense*, and *M. bolletii* that is not observed when ZF are infected with *M. marinum* or *M. chelonae*, an RGM phylogenetically related to *M. abscessus*, suggesting that this pathophysiological trait is specific for the *M. abscessus* complex. Abscesses in the CNS developed rapidly and were followed by larval death. This observation is of particular interest in light of recent clinical reports of human patients with *M. abscessus* infections in the CNS (39, 40). Interestingly, in ZF embryos the colonization of the CNS by infected macrophages coincides with the appearance of the microglia, the resident brain macrophages (41). Therefore, one could hypothesize that the source of the brain infection is the circulating, bacteria-containing macrophages that enter the CNS from the blood stream and differentiate into microglial cells. The neurotropic behavior we found has been completely overlooked in all previous studies, although more than 50 y ago Runyon observed the neurological disorder termed "spinning disease" in mice infected i.v. with the *M. abscessus* R variant (42). This observation provides additional evidence of the potential of the ZF model for studying *M. abscessus* pathogenesis.

GPLs are required for sliding motility and biofilm formation (43, 44). The *mmpL4b* protein is involved in translocation of GPLs to the bacterial surface, and its absence leads to the loss of GPLs and to the highly virulent R morphotype (14). We show here that disruption of *mmpL4b* in an S-variant background produced the pathophysiological traits of the R strain—virulence, neurotropism and cording—thus establishing the absence of GPLs as key determinant in the greater virulence of the *M. abscessus* R variant. One explanation for this greater virulence is the "unmasking" model, which proposes that the loss of GPLs could unmask lipoproteins that provoke cell-wall inflammation

(35) and/or phosphatidyl-*myo*-inositol mannosides (45), known as Toll-like receptor 2 agonists. However, this model does not completely explain the virulence of the R variant in vivo, and it is very likely that additional cell-surface components are exposed as a consequence of the lack of GPLs in the R morphotype. Further investigation is warranted to find these as-yet unidentified components and to delineate the interaction of the macrophages with the surface-exposed lipoproteins and their role in granuloma formation.

Cord formation correlates with extracellular replication of mycobacteria and has been proposed as an important virulence factor of *M. tuberculosis* (46); it sometimes can be observed in sputum smears from tuberculosis patients with severe lung cavitation. Most authors, focusing on the complex network of interactions between intracellular mycobacteria and macrophages, have neglected or underestimated the role of extracellular mycobacteria in pathogenesis (47). We show here that massive cording of the *M. abscessus* R variant occurs in vivo, but although the number and size of cords increased over time within the CNS, they remained constant within the vasculature, perhaps because of a more dynamic and efficient containment of cords by circulating macrophages. Macrophage depletion dramatically accelerated extracellular growth, as evidenced by massive and rapid cord formation in the vasculature, leading to early larval death at 3 dpi. *Pseudomonas*, *Staphylococcus*, and other related microorganisms infecting CF patients previously have been considered to be exclusively extracellular pathogens. The rapidly growing phagocytosis-resistant *M. abscessus* cords also may favor colonization and tissue damage. Several epidemiological studies have reported more frequent persistence of the R morphotype in CF patients (4) as well as an association of *M. abscessus* R with acute respiratory distress syndrome (11).

Recent elegant studies suggested that size is a determining factor for an infectious agent's success, and many successful pathogens have evolved strategies to modulate their effective size to accommodate these challenges (48, 49). Morphological plasticity can be viewed as a mechanism used by bacterial

pathogens to subvert host immunity (50). We demonstrate here that cording prevents predation by neutrophils and macrophages, presumably because the extremely long serpentine cords exceed the capacity of the professional phagocytes to surround and internalize them. Thus, cording represents an example of morphological plasticity, and inhibiting cord formation and thereby precluding the establishment of a lethal infection could be a therapeutic or prophylactic strategy.

We anticipate that the genes required for cording are unique to *M. abscessus* and are different from those in *M. tuberculosis*. In *M. tuberculosis* and *Mycobacterium bovis* bacillus Calmette–Guérin, the cyclopropane synthase PcaA is required for cording (46, 51), but our preliminary analysis suggests that *M. abscessus* mycolic acids are not cyclopropanated. If the determinants controlling cording in *M. abscessus* can be identified, they could be attractive drug targets for an innovative therapeutic approach. *M. abscessus* is responsible for more than 80% of all pulmonary infections caused by RGM in the United States and is associated with a much higher fatality rate than any other RGM (52), perhaps because it also is the most innately antibiotic-resistant RGM species (1). Although *M. abscessus* infections are more common in patients with underlying pulmonary pathology, ~30% of cases occur in apparently healthy subjects (52). In recent years the frequency and severity of pulmonary infections caused by the *M. abscessus* complex in CF patients has been well established (3, 5, 53), but very little is known about the mechanisms that give the *M. abscessus* R variant an advantage in resisting the hostile CF lung environment, where inflammation and oxygen radicals are capable of inhibiting colonization by most other bacteria. Accumulation of the particular bronchial mucus associated with the CF transmembrane conductance regulator (CFTR) defect allows bacteria such as *Pseudomonas aeruginosa* or *M. abscessus* to col-
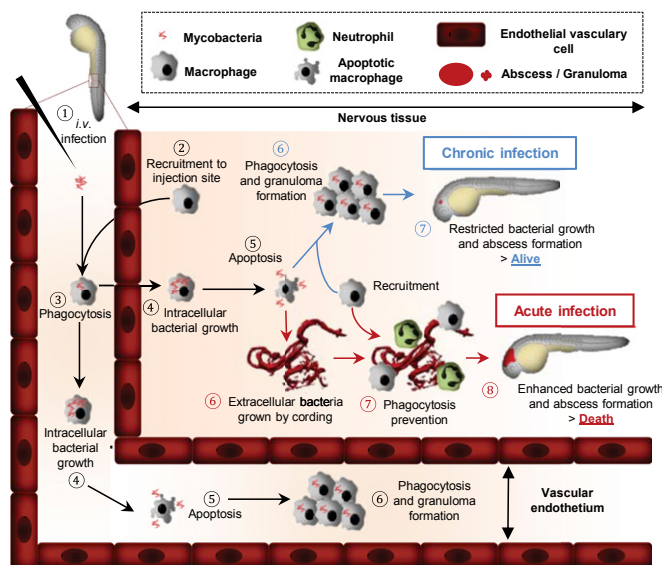
Fig. 8. Modeling the physiopathology of *M. abscessus* in ZF embryos. After injection in the blood flow (1), *M. abscessus* are rapidly engulfed by macrophages attracted by chemotaxis to the injection site (2 and 3). Infected macrophages migrate from the vasculature to the nervous tissues, become heavily infected (4), and eventually die (5). Apoptosis leads to the release of S variants (blue pathway) that subsequently are phagocytosed by newly recruited macrophages to form cellular aggregates (6). Bacterial multiplication is controlled, and a chronic infection is established. For the *M. abscessus* R variant (red pathway), apoptosis correlates with the appearance of extracellular serpentine cords (6), preventing phagocytosis by macrophages and neutrophils (7), leading to unrestricted cording, abscess formation with tissue destruction, and larval death (8).
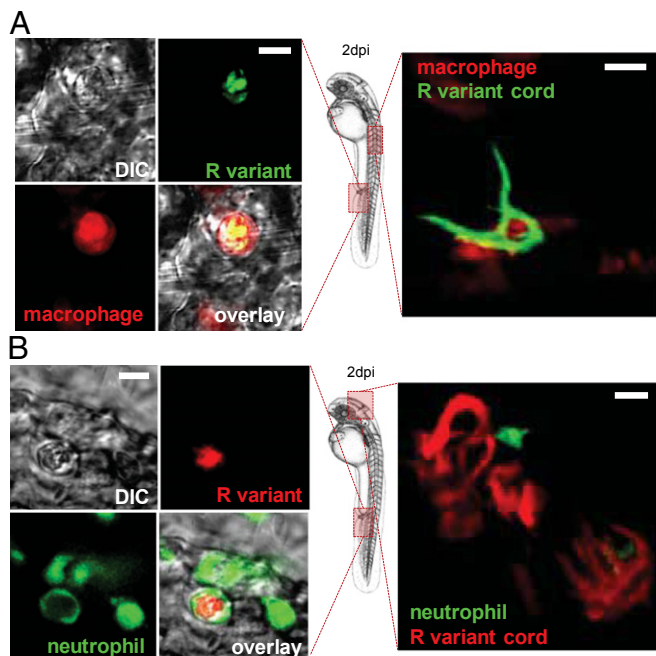
onize CF lungs. When *P. aeruginosa* colonizes CF lungs, it tends to change its phenotype, as does *M. abscessus*, although in contrast to *M. abscessus*, *P. aeruginosa* becomes more mucoid (54, 55). *Cftr* transcripts are expressed in ZF macrophages and neutrophils, and ZF *cftr* morphants, produced by a targeted knockdown of *cftr*, exhibit a reduced respiratory burst response and an increased bacterial load following *P. aeruginosa* infection (56), thus supporting a connection between *cftr* and innate immunity. Whether this CFTR defect in ZF also favors the colonization by and persistence of *M. abscessus* remains to be addressed.

In conclusion, we have shown that the *M. abscessus*/ZF system is a tractable and faithful model that can be used to unravel the events characterizing infection with *M. abscessus*, which is now considered a human pathogen. The ZF model is particularly suited for high-throughput in vivo screening (57) to find new drugs active against this highly resistant and problematic mycobacterium.

Methods

Bacterial Strains and Growth Conditions. Bacterial strains, mutants, and plasmids used for this study are described in Table S1. Mycobacteria were grown at 30 °C in Middlebrook 7H9 broth supplemented with 10% (vol/vol) oleic acid/albumin/dextrose/catalase (OADC) enrichment and 0.05% Tween 80 or on 7H10 agar containing 10% (vol/vol) OADC with appropriate antibiotics at following concentrations: kanamycin 250 μg/mL, hygromycin 250 μg/mL or zeocin 100 μg/mL. For cloning, *Escherichia coli* strain Top10 was used and grown at 37 °C in LB medium with kanamycin (25 μg/mL), hygromycin (25 μg/mL), or zeocin (25 μg/mL) when required.

Plasmid Constructions and DNA Manipulations. Versions of integrative or replicative plasmids to allow selection on zeocin were generated (Table S1). The kanamycin cassette of pMV306 (58) was replaced with the zeocin cassette, which was amplified from pCR-BluntII-TOPO (Invitrogen) using the primers Zeo-up (5′-AAA GCT AGC TTA CAA TTT CCT GAT G-3′; NheI underlined) and Zeo-lo (5′-AAC TAG TCA GTC CTG CTC CTC G-3′; SpeI underlined) and ligated into the NheI/SpeI-restricted pMV306 product to generated

Fig. 7. In vivo cording of the R variant prevents phagocytosis. (*A*) *Tg(mpeg1:mCherry)* embryos harboring red-fluorescent macrophages were infected with GFP-expressing R variants. (*Left*) Maximum intensity projection of confocal images of macrophages capable of phagocytosing the *M. abscessus* R variant in the vascular system. (*Right*) Macrophages are unable to internalize *M. abscessus* R cords. (Scale bars, 10 μm.) (*B*) *Tg(mpx:egfp)* embryos harboring green-fluorescent neutrophils were infected with mCherry-expressing R variants. (*Left*) Maximum intensity projection of confocal images of *M. abscessus* R-variant internalized neutrophils in the vascular system. (Scale bar, 10 μm). (*Right*) Neutrophils are unable to internalize *M. abscessus* R-variant cords. (Scale bars, 15 μm.)

pMV306_zeo. The p MV261_zeo was generated by replacing the kanamycin cassette of pMV261 with the zeocin cassette, which was excised from pMV306_zeo following restriction with NheI and SpeI and subsequently was ligated into the NheI/SpeI-digested pMV261. The same cloning strategy was used to generate pMV261_mCherry_zeo derived from the pMV261_mCherry (24). Integrative expression of *gfp* was performed by cloning the XbaI/HindIII fragment of pVV16 containing the constitutive *hsp60* promoter coupled with the *eGFP* gene into the XbaI/HindIII digested pMV306_zeo, resulting in pMV306_eGFP_zeo. Restriction enzymes and T4 DNA ligase were from New England Biolabs, and Goldstar DNA polymerase was from Eurogentec.

ZF Care, Strains, and Maintenance. All animal experiments were conducted at the University Montpellier 2 according to European Union guidelines for handling of laboratory animals and were approved by the Direction Sanitaire et Vétérinaire de l'Hérault and Comité d'Ethique pour l'Expérimentation Animale under reference CEEA-LR-13007. Experiments were performed using the *golden* ZF mutant (59) or the following transgenic lines: tg(*mpx:egfp*) (60), tg(*kdr:egfp*) (61), and tg(*mpeg1:mCherry*) (this study, see below). Eggs were obtained by natural spawning and incubated at 28.5 °C in water with 60 μg/mL ocean salts. Embryo age is expressed as hpf or days post fertilization.

Generation of the Transgenic *mpeg1:mCherry* Line. The *mpeg1* promoter used to drive the specific expression of membrane-targeted RFP in macrophages was amplified using primers zMpeg1P4 5′-TTGGAGCACATCTGAC-3′ and zMpeg1E2N2 5′-TTATAGCGGCCGCGAAATGCTCTTGACTTCATGA-3′, digested by NotI, and ligated to the coding phase of the farnesylated mCherry protein so that the Mpeg1 AUG is in phase with the downstream mCherry-F ORF on a Tol2-derived vector (GenBank accession no. GU394080). The resulting plasmid together with the Transposase mRNA was injected into embryos at the one-cell stage.

Microinjection of Mycobacteria into ZF Embryos. Mycobacterial strains expressing mCherry, tdTomato, or GFP were grown to midlog phase and recovered by centrifugation, washed twice, and resuspended in PBS supplemented with 0.05% Tween-80 (PBS^T). Bacterial suspensions were homogenized through a 26-gauge needle and sonicated three times for 10 s each to disperse bacteria. Any remaining clump was allowed to settle for 5–10 min. Microscopic examination of the bacterial suspensions revealed the presence of highly homogenous preparations consisting mainly of individualized bacilli with no bacterial clumps or cords that would prevent subsequent microinjections. Supernatants were resuspended at an OD_{600} of 1 in PBS^T with phenol red. Infection was carried by microinjection of ∼2–3 nL of bacterial suspensions, containing 150–300 bacteria, into the caudal vein of dechorionated and anesthetized embryos at 30 hpf. To follow infection kinetics, infected larvae were transferred into individual wells and incubated at 28.5 °C. The inoculum size was checked a posteriori by injection in sterile PBS^T and plating on 7H10 agar containing 10% (vol/vol) OADC and appropriate antibiotics. Survival curves were established by counting dead embryos (no heartbeat) every day, up to 13 d.

Microinjection of Lipo-Clodronate into Embryos. For the selective depletion of macrophages into embryos, liposome-encapsulated clodronate or Lipo-clodronate (Lipo-C) and liposome-encapsulated PBS (Lipo-PBS) for control were obtained from David A. Mancardiand (Pasteur Institute, Paris) and prepared as previously described (36). Embryos injected with Lipo-PBS or Lipo-C injected were generated by the microinjection of 2–3 nL of the suspension into the caudal vein of tg(*mpeg1:mCherry*) embryos, previously dechorionated and anesthetized with 0.02% tricaine, at 24 hpf. Proper depletion of macrophages in Lipo-C–injected embryos was compared with Lipo-PBS–injected embryos (control) and subsequently was confirmed by fluorescent microscopy.

Bacterial Loads in Infected Embryos. Groups of three infected embryos were collected, lysed individually in 2% (vol/vol) Triton X-100 PBS^T, homogenized with a 26-gauge needle, and resuspended in PBS^T. Several dilutions of homogenates were plated on Middlebrook 7H10/OADC and supplemented with BBL MGIT PANTA (BD) as recommended by the supplier. Cfu were determined at 0, 3, 5, and 7 dpi.

Microinjection of Morpholinos. A mix of splice-blocking 5′-GGTCTTTCTCCTTAC-CATGTCTCC-3′ and ATG 5′-CCTCCATTCTGTACGGATGCAGCAT-3′ morpholinos against *pu.1* gene were purchased from Gene Tools and combined as described (37). The morpholino mix was prepared in morpholino buffer containing 10% (vol/vol) phenol red, and 3 nL was injected into one-cell-stage *mpeg1:mCherry* and *mpx:egfp* ZF. The proper depletion of macrophages, but not of neutrophils, in *pu.1* morphants was confirmed by fluorescent microscopy.

Microscopy. Wide-field, bright-field, and fluorescence live microscopy of infected embryos were performed using an Olympus MVX10 epifluorescent microscope equipped with a X-Cite120Q (Lumen Dynamics) 120-W mercury light source. Images were acquired with a digital color camera (Olympus XC50) and processed using CellSens (Olympus). Fluorescence filters cubes (FITC-MVX10 and TRITC-MVX10) were used to detect green and red light, respectively. Confocal fluorescence microscopy was performed using a Leica DM2500CSQ upright microscope with a Leica TCS SPE confocal scan head, differential interference contrast (DIC) optics, and a SuperZGalvo SPE z-step controller. GFP and mCherry were excited with either a Leica EL6000 120-W mercury lamp or 488-nm and 532-nm lasers. Wide-field fluorescence and DIC images were captured by LAS-AF software (Leica Microsystems). For fixed-sample observations, animals in 50% (vol/vol) glycerol in PBS were mounted flat onto depression transparent slides with a coverslip and observed with a 10× Leica Apo 0.3 NA, 40× Leica Apo oil 1.15 NA, or 63× Leica Apo oil 1.33 NA objective. For live imaging, anesthetized infected embryos were positioned in dishes and immobilized with 1% low-melting-point agarose covering the entire larva. Immobilized embryos were immersed with fish water containing tricaine for direct visualization using 20× Leica Apo water 0.5 NA or 40× Leica Apo water 0.8 NA objectives.

Image Processing and Analysis. Overlays of fluorescent and DIC images and 2D reconstructions of image stacks were processed and assembled using LAS-AF software. 3D volume reconstitution was produced using Imaris 7.0 software (Bitplane). Movies were generated from compiled image stacks using Imaris 7.0 software and were exported as AVI files. Final image analysis and visualization were performed using GIMP 2.6 freeware or Imaris 7.0 software to adjust levels and brightness and to remove out-of-focus background fluorescence.

Histochemistry and Vital Dye Staining of Embryos. Anesthetized embryos were fixed overnight at 4 °C in 4% (vol/vol) paraformaldehyde in PBS, then were washed twice in PBS, and were transferred gradually from PBS to 50% (vol/vol) glycerol for microscopic observation. For electron microscopy, embryos were fixed and processed as described previously (62). For the detection of apoptotic cells, living embryos were soaked in 5 μg/mL AO in fish water for 30 min, rinsed twice, and incubated at 28.5 °C.

Statistical Analyses. Statistical analyses of comparisons between survival curves were performed using the log rank test with Prism 4.0 (GraphPad, Inc.). Quantification experiments were analyzed by EcoStats Company (http://ecostats34.free.fr) using generalized mixed-effects models performed with R 2.14.1 (R Development Core Team 2011) and with Excel 2010 (Microsoft). Statistical significance was assumed at P values <0.05.

1. Brown-Elliott BA, Wallace RJ, Jr. (2002) Clinical and taxonomic status of pathogenic non-pigmented or late-pigmenting rapidly growing mycobacteria. *Clin Microbiol Rev* 15(4): 716–746.
2. Wallace RG, Jr., Silcox V, Brown BA (1994) Taxonomy of rapidly growing mycobacteria. *Clin Infect Dis* 18(1):121–122.
3. Olivier KN, et al.; Nontuberculous Mycobacteria in Cystic Fibrosis Study Group (2003) Nontuberculous mycobacteria. I: Multicenter prevalence study in cystic fibrosis. *Am J Respir Crit Care Med* 167(6):828–834.
4. Jönsson BE, et al. (2007) Molecular epidemiology of *Mycobacterium abscessus*, with focus on cystic fibrosis. *J Clin Microbiol* 45(5):1497–1504.
5. Roux AL, et al.; Jean-Louis Herrmann for the OMA Group (2009) Multicenter study of prevalence of nontuberculous mycobacteria in patients with cystic fibrosis in france. *J Clin Microbiol* 47(12):4124–4128.
6. Sermet-Gaudelus I, et al. (2003) *Mycobacterium abscessus* and children with cystic fibrosis. *Emerg Infect Dis* 9(12):1587–1591.
7. Medjahed H, Gaillard JL, Reyrat JM (2010) *Mycobacterium abscessus*: A new player in the mycobacterial field. *Trends Microbiol* 18(3):117–123.
8. Byrd TF, Lyons CR (1999) Preliminary characterization of a *Mycobacterium abscessus* mutant in human and murine models of infection. *Infect Immun* 67(9): 4700–4707.

9. Catherinot E, et al. (2007) Hypervirulence of a rough variant of the *Mycobacterium abscessus* type strain. *Infect Immun* 75(2):1055–1058.

10. Cullen AR, Cannon CL, Mark EJ, Colin AA (2000) *Mycobacterium abscessus* infection in cystic fibrosis. Colonization or infection? *Am J Respir Crit Care Med* 161(2 Pt 1): 641–645.

11. Catherinot E, et al. (2009) Acute respiratory failure involving an R variant of *Mycobacterium abscessus*. *J Clin Microbiol* 47(1):271–274.

12. Howard ST, et al. (2006) Spontaneous reversion of *Mycobacterium abscessus* from a smooth to a rough morphotype is associated with reduced expression of glycopeptidolipid and reacquisition of an invasive phenotype. *Microbiology* 152(Pt 6): 1581–1590.

13. Cortes M, et al. (2011) Conditional gene expression in *Mycobacterium abscessus*. *PLoS ONE* 6(12):e29306.

14. Medjahed H, Reyrat JM (2009) Construction of *Mycobacterium abscessus* defined glycopeptidolipid mutants: Comparison of genetic tools. *Appl Environ Microbiol* 75(5):1331–1338.

15. Ripoll F, et al. (2009) Non mycobacterial virulence genes in the genome of the emerging pathogen *Mycobacterium abscessus*. *PLoS ONE* 4(6):e5660.

16. Zerihun MA, Hjortaas MJ, Falk K, Colquhoun DJ (2011) Immunohistochemical and Taqman real-time PCR detection of mycobacterial infections in fish. *J Fish Dis* 34(3): 235–246.

17. Jacobs JM, Stine CB, Baya AM, Kent ML (2009) A review of mycobacteriosis in marine fish. *J Fish Dis* 32(2):119–130.

18. Kang GC, Gan AW, Yam A, Tan AB, Tay SC (2010) *Mycobacterium abscessus* Hand infections in immunocompetent fish handlers: Case Report. *J Hand Surg Am* 35(7): 1142–1145.

19. Davis JM, et al. (2002) Real-time visualization of mycobacterium-macrophage interactions leading to initiation of granuloma formation in zebrafish embryos. *Immunity* 17(6):693–702.

20. van der Sar AM, Appelmelk BJ, Vandenbroucke-Grauls CM, Bitter W (2004) A star with stripes: Zebrafish as an infection model. *Trends Microbiol* 12(10):451–457.

21. Clay H, Volkman HE, Ramakrishnan L (2008) Tumor necrosis factor signaling mediates resistance to mycobacteria by inhibiting bacterial growth and macrophage death. *Immunity* 29(2):283–294.

22. Prajsnar TK, Cunliffe VT, Foster SJ, Renshaw SA (2008) A novel vertebrate model of *Staphylococcus aureus* infection reveals phagocyte-dependent resistance of zebrafish to non-host specialized pathogens. *Cell Microbiol* 10(11):2312–2325.

23. Levraud JP, et al. (2009) Real-time observation of *listeria monocytogenes*-phagocyte interactions in living zebrafish larvae. *Infect Immun* 77(9):3651–3660.

24. Alibaud L, et al. (2011) A *Mycobacterium marinum* TesA mutant defective for major cell wall-associated lipids is highly attenuated in *Dictyostelium discoideum* and zebrafish embryos. *Mol Microbiol* 80(4):919–934.

25. Vergunst AC, Meijer AH, Renshaw SA, O'Callaghan D (2010) *Burkholderia cenocepacia* creates an intramacrophage replication niche in zebrafish embryos, followed by bacterial dissemination and establishment of systemic infection. *Infect Immun* 78(4):1495–1508.

26. Berg RD, Ramakrishnan L (2012) Insights into tuberculosis from the zebrafish model. *Trends Mol Med* 18(12):689–690.

27. Tobin DM, et al. (2010) The *lta4h* locus modulates susceptibility to mycobacterial infection in zebrafish and humans. *Cell* 140(5):717–730.

28. Davis JM, Ramakrishnan L (2009) The role of the granuloma in expansion and dissemination of early tuberculous infection. *Cell* 136(1):37–49.

29. Adams KN, et al. (2011) Drug tolerance in replicating mycobacteria mediated by a macrophage-induced efflux mechanism. *Cell* 145(1):39–53.

30. Volkman HE, et al. (2004) Tuberculous granuloma formation is enhanced by a *mycobacterium* virulence determinant. *PLoS Biol* 2(11):e367.

31. Adékambi T, et al. (2004) Amoebal coculture of "*Mycobacterium massiliense*" sp. nov. from the sputum of a patient with hemoptoic pneumonia. *J Clin Microbiol* 42(12):5493–5501.

32. Adékambi T, Berger P, Raoult D, Drancourt M (2006) rpoB gene sequence-based characterization of emerging non-tuberculous mycobacteria with descriptions of *Mycobacterium bolletii* sp. nov., *Mycobacterium phocaicum* sp. nov. and *Mycobacterium aubagnense* sp. nov. *Int J Syst Evol Microbiol* 56(Pt 1):133–143.

33. Sánchez-Chardi A, et al. (2011) Demonstration of cord formation by rough *Mycobacterium abscessus* variants: Implications for the clinical microbiology laboratory. *J Clin Microbiol* 49(6):2293–2295.

34. Pawlik A, et al. (2013) Identification and characterization of the genetic changes responsible for the characteristic smooth-to-rough morphotype alterations of clinically persistent *Mycobacterium abscessus*. *Mol Microbiol* 90(3):612–629.

35. Roux AL, et al. (2011) Overexpression of proinflammatory TLR-2-signalling lipoproteins in hypervirulent mycobacterial variants. *Cell Microbiol* 13(5):692–704.

36. Van Rooijen N, Sanders A (1994) Liposome mediated depletion of macrophages: Mechanism of action, preparation of liposomes and applications. *J Immunol Methods* 174(1-2):83–93.

37. Clay H, et al. (2007) Dichotomous role of the macrophage in early *Mycobacterium marinum* infection of the zebrafish. *Cell Host Microbe* 2(1):29–39.

38. Cosma CL, Klein K, Kim R, Beery D, Ramakrishnan L (2006) *Mycobacterium marinum* Erp is a virulence determinant required for cell wall integrity and intracellular survival. *Infect Immun* 74(6):3125–3133.

39. Talati NJ, Rouphael N, Kuppalli K, Franco-Paredes C (2008) Spectrum of CNS disease caused by rapidly growing mycobacteria. *Lancet Infect Dis* 8(6):390–398.

40. Lee MR, et al. (2012) CNS infections caused by *Mycobacterium abscessus* complex: Clinical features and antimicrobial susceptibilities of isolates. *J Antimicrob Chemother* 67(1):222–225.

41. Herbomel P, Thisse B, Thisse C (1999) Ontogeny and behaviour of early macrophages in the zebrafish embryo. *Development* 126(17):3735–3745.

42. Runyon EH (1959) Anonymous mycobacteria in pulmonary disease. *Med Clin North Am* 43(1):273–290.

43. Recht J, Martínez A, Torello S, Kolter R (2000) Genetic analysis of sliding motility in *Mycobacterium smegmatis*. *J Bacteriol* 182(15):4348–4351.

44. Recht J, Kolter R (2001) Glycopeptidolipid acetylation affects sliding motility and biofilm formation in *Mycobacterium smegmatis*. *J Bacteriol* 183(19):5718–5724.

45. Rhoades ER, et al. (2009) *Mycobacterium abscessus* Glycopeptidolipids mask underlying cell wall phosphatidyl-myo-inositol mannosides blocking induction of human macrophage TNF-alpha by preventing interaction with TLR2. *J Immunol* 183(3): 1997–2007.

46. Glickman MS, Cox JS, Jacobs WR, Jr. (2000) A novel mycolic acid cyclopropane synthetase is required for cording, persistence, and virulence of *Mycobacterium tuberculosis*. *Mol Cell* 5(4):717–727.

47. Grosset J (2003) *Mycobacterium tuberculosis* in the extracellular compartment: An underestimated adversary. *Antimicrob Agents Chemother* 47(3):833–836.

48. Weiser JN (2013) The battle with the host over microbial size. *Curr Opin Microbiol* 16(1):59–62.

49. Justice SS, Hunstad DA, Cegelski L, Hultgren SJ (2008) Morphological plasticity as a bacterial survival strategy. *Nat Rev Microbiol* 6(2):162–168.

50. Horvath DJ, Jr., et al. (2011) Morphological plasticity promotes resistance to phagocyte killing of uropathogenic Escherichia coli. *Microbes Infect* 13(5):426–437.

51. Corrales RM, et al. (2012) Phosphorylation of mycobacterial PcaA inhibits mycolic acid cyclopropanation: Consequences for intracellular survival and for phagosome maturation block. *J Biol Chem* 287(31):26187–26199.

52. Griffith DE, Girard WM, Wallace RJ, Jr. (1993) Clinical features of pulmonary disease caused by rapidly growing mycobacteria. An analysis of 154 patients. *Am Rev Respir Dis* 147(5):1271–1278.

53. Pierre-Audigier C, et al. (2005) Age-related prevalence and distribution of non-tuberculous mycobacterial species among patients with cystic fibrosis. *J Clin Microbiol* 43(7):3467–3470.

54. Govan JR, Deretic V (1996) Microbial pathogenesis in cystic fibrosis: Mucoid *Pseudomonas aeruginosa* and *Burkholderia cepacia*. *Microbiol Rev* 60(3):539–574.

55. Govan JR, Fyfe JA (1978) Mucoid *Pseudomonas aeruginosa* and cystic fibrosis: Resistance of the mucoid from to carbenicillin, flucloxacillin and tobramycin and the isolation of mucoid variants in vitro. *J Antimicrob Chemother* 4(3):233–240.

56. Phennicie RT, Sullivan MJ, Singer JT, Yoder JA, Kim CH (2010) Specific resistance to *Pseudomonas aeruginosa* infection in zebrafish is mediated by the cystic fibrosis transmembrane conductance regulator. *Infect Immun* 78(11):4542–4550.

57. Takaki K, Cosma CL, Troll MA, Ramakrishnan L (2012) An *in vivo* platform for rapid high-throughput antitubercular drug discovery. *Cell Rep* 2(1):175–184.

58. Stover CK, et al. (1991) New use of BCG for recombinant vaccines. *Nature* 351(6326): 456–460.

59. Lamason RL, et al. (2005) SLC24A5, a putative cation exchanger, affects pigmentation in zebrafish and humans. *Science* 310(5755):1782–1786.

60. Renshaw SA, et al. (2006) A transgenic zebrafish model of neutrophilic inflammation. *Blood* 108(13):3976–3978.

61. Jin SW, Beis D, Mitchell T, Chen JN, Stainier DY (2005) Cellular and molecular analyses of vascular tube and lumen formation in zebrafish. *Development* 132(23):5199–5209.

62. Giffard-Mena I, Charmantier G, Grousset E, Aujoulat F, Castille R (2006) Digestive tract ontogeny of *Dicentrarchus labrax*: Implication in osmoregulation. *Dev Growth Differ* 48(3):139–151.